Journal of Geotechnical and Geoenvironmental Engineering

Modeling the Stress-Dilatancy Relationship of Unsaturated Silica Sand in Triaxial Compression Tests

--Manuscript Draft--

Manuscript Number:	GTENG-5233R2
Full Title:	Modeling the Stress-Dilatancy Relationship of Unsaturated Silica Sand in Triaxial Compression Tests
Manuscript Region of Origin:	UNITED KINGDOM
Article Type:	Technical Paper
Funding Information:	Schweizerischer Nationalfonds zur Förderung der Wissenschaftlichen Forschung (CH) (P1SKP2 158621) — Mr Elliot James Fern Seventh Framework Programme (BE) (PIAP-GA-2012-324522) — Not applicable
Abstract:	It is well known that partial saturation increases the shear strength and dilatancy of unsaturated sand. However, little research has been carried out on the actual stress-dilatancy relationship. This paper shows that the increase in peak shear strength caused by partial saturation is consistent with an increase in dilatancy and that conventional stress-dilatancy theories are still valid for unsaturated sand. The use of state indexes as a proxy for dilatancy were investigated and extended to unsaturated sands. Additionally, these indexes can be used to establish a critical state line based on material properties only. The validity of the stress-dilatancy theories and the use of state indexes offer simplicity in modeling the shear behavior of unsaturated sand. This will be demonstrated in this paper with the Nor-Sand model, and with which the wetting collapse can be explained as a consequence of a loss of dilatancy characteristics.
Corresponding Author:	Elliot James Fern, MSc University of Cambridge Cambridge, UNITED KINGDOM
Corresponding Author E-Mail:	jf497@cam.ac.uk;james.fern@bluewin.ch
Order of Authors:	Elliot James Fern, MSc Dilan Jeyachandran Robert, PhD Kenichi Soga, PhD
Additional Information:	
Question	**Response**
Is the article being considered for more than one journal? The Journal of Geotechnical and Geoenvironmental Engineering does not review manuscripts that are being submitted simultaneously to another organization or ASCE journal for publication.	No
Is this article already published? Material that has been previously published cannot be considered for publication by ASCE. A manuscript that has been published in a conference proceedings may be reviewed for publication only if it has been significantly revised. If you answer YES, please provide further explanation in your cover	No

letter.	
Have all the authors contributed to the study and approved the final version? All authors must have contributed to the study, seen the final draft of the manuscript, and accept responsibility for its contents. It is unethical to list someone as a coauthor who does not want to be associated with the study and who has never seen the manuscript.	Yes
Was an earlier version of the paper previously considered and declined by ASCE? Declined manuscripts are sent through the review process again. If your manuscript has been submitted to us before under a different title, please provide that title in the space provided below. It is our policy to inform an editor that a manuscript has been previously reviewed, even when it has been reviewed by a different Division, Institute, or Council within ASCE.	No
Do your table titles/figure captions cite other sources? If you used a figure/table from another source, written permission for print and online use must be attached in PDF format. Permission letters must state that permission is granted in both forms of media. If you used data from another source to create your own figure/table, the data is adapted and therefore obtaining permission is not required.	No
Does your paper exceed 10,000 words? If YES, please provide justification in your cover letter. If you need help estimating word length, see our sizing worksheet at this link: Sizing Worksheet. If you have questions about the Sizing Worksheet, please see the Sizing Worksheet Instructions.	No
Estimates for color figures in the printed journal begin at $924. Cost increases depend on the number and size of figures. Do you intend for any figure to be printed in color? If YES, how many and which ones? Please provide a total count and also list them by figure number.	No
Is this manuscript a companion to one already submitted/or being submitted? If yes, please note whether this is part I, II, or III. Please make sure all related papers are uploaded on the same day and provide the date of submission, title, and authors of each.	No

Is this manuscript part of a Special Issue? If yes, please provide the Special Issue title and name of the guest editor.	No
Did you include your ASCE Membership credentials in your author byline?	No
To read ASCE's Data Sharing Policy, please click on the "Instructions" link associated with this question. According to this policy, you are required to report on any materials sharing restrictions in your cover letter. Are you restricted from sharing your data & materials? If yes, did you report on these in your cover letter?	No

Modeling the Stress-Dilatancy Relationship of Unsaturated Silica Sand in Triaxial Compression Tests

Elliot James Fern[1], Not a Member, ASCE

Dilan Jeyachandran Robert [2], Not a Member, ASCE

Kenichi Soga [1], Member, ASCE

ABSTRACT

It is well known that partial saturation increases the shear strength and dilatancy of unsaturated sand. However, little research has been carried out on the actual stress-dilatancy relationship. This paper shows that the increase in peak shear strength caused by partial saturation is consistent with an increase in dilatancy, and that conventional stress-dilatancy theories are still valid for unsaturated sand. The use of state indexes, as a proxy for dilatancy, were investigated and extended to unsaturated sands. Additionally, these indexes can be used to establish a critical state line which is based on material properties only. The validity of the stress-dilatancy theories and the use of state indexes offer simplicity in modeling the shear behavior of unsaturated sand. This will be demonstrated in this paper with the Nor-Sand model, and with which the wetting collapse can be explained as a consequence of a loss of dilatancy characteristics.

Keywords: Stress-dilatancy theory, critical state theory, state indexes, unsaturated sand, constitutive modeling.

INTRODUCTION

Since the early work of Taylor (1948), it has been recognized that the development of the shear strength is a consequence of grains interlocking and the critical state strength, which was shown by Roscoe et al. (1958) to be uniquely defined. Roscoe and Schofield (1963) were driven by this idea and expressed Taylor's stress-dilatancy theory in terms of stress invariants. However, it was

[1]Dept. of Engrg., Univ. of Cambridge, Trumpington St., Cambridge CB2 1PZ, United Kingdom. E-mail: jf497@cam.ac.uk.

[2]Sch. of Civ. Env. and Chem. of Engrg., RMIT Univ., GPO Box 2476, Melbourne VIC 3001, Australia

later recognized that the contribution of dilatancy, or interlocking, was not as significant as was previously believed (*i.e.* Bolton 1986; Stroud 1971). Amongst others, Nova (1982) introduced a dilatancy parameter to minimize the influence of dilatancy on the shear strength (Eq. 1).

$$\eta' = M + (N - 1)D \tag{1}$$

where $\eta' = q/p'$ is the effective stress ratio with q the deviatoric stress and p' the mean effective stress, M the critical state stress ratio, N the dilatancy parameter and $D = \frac{d\varepsilon_v^p}{d\varepsilon_d^p}$ the dilatancy rate, $d\varepsilon_v^p$ and $d\varepsilon_d^p$, respectively, the plastic volumetric and deviatoric strain increments.

Roscoe and Schofield (1963) established the Original Cam-Clay model from the stress-dilatancy theory by assuming that the development of plastic volumetric strains followed the development of the shear strength. In turn, Roscoe and Burland (1968) simplified the equation to formulate the Modified Cam-Clay model. Roscoe (1970) later recognized the limitations of these models in predicting the behavior of sand, and the necessity of introducing a hardening law based on a strain invariant which would relate to the critical state. Jefferies (1993) suggested using the state parameter (Been and Jefferies 1985) as a strain invariant (Eq. 2).

$$\psi = e - e_{cs} \tag{2}$$

where ψ is the state parameter, e the void ratio and e_{cs} the critical state void ratio.

The state parameter is a measurement of how much the sand has to contract or dilate in order to reach the critical state. Jefferies (1993) then derived Nova's stress-dilatancy rule (Eq. 1) to formulate the Nor-Sand model which, unlike the Cam-Clay models, included the void ratio as a model variable. It also allowed plasticity to take place prior to the peak state.

The idea of introducing plasticity before the peak state was not new (Drucker et al. 1957). Dafalias and Popov (1975) introduced it in a bounding surface model for cyclic loading, and Bardet (1986) for triaxial loading. Hashiguchi and Chen (1998) introduced the sub-loading surface concept, which also allowed plasticity to take place prior to the peak state by reformulating the consistency condition. This allowed existing models, such as the Cam-Clay models, to be updated. Nor-Sand resembles these models in the sense that it predicts the hardening rate by comparing the current stress state with an estimated peak state.

Despite the fact that all Cambridge-type theories and models originate from the stress-dilatancy theory, it is surprising that little attention has been given to these relationships when modeling the behavior of partially saturated soils. Alonso et al. (1990) carried out a straightforward extension of the modified Cam-Clay model for unsaturated soils by introducing the loading-collapse (LC) curve. However, it did not include sub-loading surface and hence plasticity prior to the peak state. The LC curve enhanced the preconsolidation pressure with partial saturation. Therefore, it assumed that the peak strength was a yielding point which violates the stress dilatancy theory. Cui and Delage (1996) also observed the enhancement by partial saturation of both the peak strength and the dilatancy rates. However, they still considered the peak state as a yielding point and, consequently, suggested a different shape of the yield surface to accommodate this modeling assumption. Chiu and Ng (2003) understood the importance of the stress-dilatancy theory in developing new stress-strain relationships for unsaturated sand, and proposed a model which would capture the peak strength as a consequence of dilatancy. However, this model was developed on mildly dilative soils, which did not offer sufficient data to extend any state index (Ng and Menzies 2007). Russell and Khalili (2006) suggested a bounding surface model for both unsaturated clays and sands, which allowed plasticity to take place prior to the peak and was able to predict wetting-collapses without introducing a loading-collapse curve. Many of the available models show good abilities in modeling the behavior of unsaturated soils (D'Onza et al. 2011). However, these models relied on a vast number of model parameters, which do not necessarily have any physical meaning or are not easily quantifiable.

This paper aims to demonstrate the validity of the stress-dilatancy theory for unsaturated sand, and explains the increase of peak strength as the consequence of an increase of the dilatancy rates. The use of state indexes as proxies for dilatancy can be extended to unsaturated sand, and can be used to predict the peak state. The ability to predict both the critical state and peak states offers simplicity in modeling the behavior of unsaturated sands, and will be demonstrated with the Nor-Sand model. It will also be shown that the on-set of a wetting collapse can be understood, and modeled as a loss of dilatancy characteristics rather than a yielding point.

CRITICAL STATE STRENGTH AND STRESS VARIABLES

The critical state theory (Roscoe et al. 1958) suggests that any soils sheared sufficiently will ultimately reach a unique state called the critical state. In this state, the soil will be continuously deformed without any changes in volume or stress state. Therefore, the stress-dilatancy theory (Eq. 1) and the state parameter (Eq. 2) at critical state yield to Eq. 3.

$$D := 0 \quad \rightarrow \quad \eta' = M, \quad \psi = 0 \tag{3}$$

Partial saturation is known to enhance the critical state strength of soil. However, its expression depends on the choice of the stress variables. There is little consensus on which variables to use. Bishop (1959) suggested a generalized formulation of Terzaghi's effective stress (Eq. 4) which directly took into account the contribution of partial saturation through suction s and a coupling parameter χ.

$$p' = p^{net} + \chi s \tag{4}$$

where p' is the mean effective stress , $p^{net} = p^{tot} - p_a$ the mean net stress with p^{tot} the mean total stress and p_a the pore air pressure, $s = p_a - p_w$ the matric suction with p_w the pore water pressure and χ the coupling parameter.

Bishop's effective stress (Eq. 4) provides a stress variable, which explains any change in strains by a change in stresses. However, the quantification of the coupling parameter χ has been a matter of debate since its original formulation (*i.e.* Aitchison 1960; Bishop and Blight 1963; Coleman 1962). Its incapacity to explain the wetting-collapse in the framework of elasticity made it unpopular (Jennings and Burland 1962), despite evidence that the wetting-collapse was a plastic behavior (Leonards 1962). It was only later that the plastic nature of the wetting-collapse reached a consensus with the introduction of the LC-curve (Alonso et al. 1990). However, the use of Bishop's effective stress was still unpopular, as it could not explain the peak strength in an elastic-plastic framework. In this context, it was acknowledge that the coupling parameter χ would mainly depend on the degree saturation S_w (Bishop and Blight 1963) but would have to include some dependency to pressure (Aitchison 1960), to the stress history (Coleman 1962), and even to the soil structure (Alonso et al. 2010). Khalili et al. (2004) pointed out that most arguments against Bishop's effective stress were formulated within the context of linear elasticity. Non-recoverable deformations, such as dilation or collapses, could not even be explained for saturated soils in terms of effective stresses alone without invoking appropriate plasticity theories. It is known for saturated sand that the peak strength is a consequence of dilatancy, and that plasticity takes place prior to the peak. Dilatancy is density and pressure dependent (Been and Jefferies 1985; Bolton 1986) and plasticity is stress path dependent. Therefore, it is believed that the only reason that the peak strength could not be predicted with Bishop's effective stress is due to limitations of the elastic-plastic modeling framework.

Khalili and Khabbaz (1998) suggested a non-linear coupling parameter χ as a function of matric suction s only, and overcame some of the historical skepticism in using Bishop's effective stress. The non-linearity was necessary as it was used to predict the peak strength in association with a Mohr-Coulomb model for unsaturated soils (Fredlund et al. 1978), which is set in the elastic-plastic framework. It can be argued that the proposed non-linear coupling parameter χ encapsulated the non-linearity present in the soil water retention curve (SWRC). However, it was later shown that this empirical relationship could be adapted to capture the critical state strength (Loret and Khalili 2000). However, the coupling parameter χ was found to be different for unsaturated clays and sands (Russell and Khalili 2006). Nuth (2009) reviewed the data of Wheeler and Sivakumar (1995), Maatouk et al. (1995), Cui and Delage (1996), Geiser (1999), Rampino et al. (2000) and Toll and Ong (2003), and showed that the critical state stress ratio M was uniquely defined when the coupling parameter χ was taken as the degree of saturation. Other authors (*i.e.* Bolzon et al. 1996; Lu and Likos 2004) suggested using the effective degree of saturation (Eq. 5) as a coupling parameter χ. Alonso et al. (2010) suggested a similar coupling parameter χ which yields to Eq. 5 for silica sand.

$$\chi = S'_w = \frac{S_w - S_{res}}{1 - S_{res}} \qquad \text{if} \quad S_w \geq S_{res} \tag{5}$$

where S'_w is the effective degree of saturation, S_w the degree of saturation and S_{res} the residual degree of saturation.

The advantage of using the effective degree of saturation S'_w instead of the degree of saturation S_w is that it avoids exponentially increasing values of suction stress ($s \cdot S'_w$) around the residual degree of saturation, whilst no affecting much the suction stress at higher degree of saturation.

CHIBA SAND

In this study, the mechanical behavior of an unsaturated silica sand, called Chiba, sand was undertaken. Chiba sand is a poorly graded silica sand with a particle size ranging from 0.01 mm to 1.00 mm. It has a coefficient of uniformity of 2.1 and a coefficient of curvature of 1.1. The grain-size distribution was obtained by sieving and sedimentation and is shown in Fig. 1(a). The minimum and maximum void ratios were found to be respectively 0.500 and 0.946, and its specific gravity 2.72. The critical state friction angle was found to be $33°$, a typical value for silica sand.

The SWRC was obtained for the drying path by Robert (2010) and for three different densities using the axis translation technique. The specimens were subjected to matric suctions of 2 to 60 kPa. Pressure ranging from 2 to 10 kPa were applied by means of negative water head (buret) and the 60 kPa with a pressure plate. Complimentary investigations were carried out on a loose specimen and the air entry value s_e, which was found to be 0.5 kPa, the residual degree of saturation around 20%, and a very small hysteresis was found. Similar results were obtained by Schnellmann et al. (2013) for Eschenbach Sand and Russell (2004) for Kurnell Sand. However, the SWRC were obtained using similar techniques which could explain similar results and high residual degree of saturation. The SWRC were fitted with a van Genuchten (1980) model (Eq. 6) for each density and the results are summarized in Table 1. Fig 1(b) shows the experimental results and model fittings.

$$S'_w = [1 + (\alpha_w s)^{n_w}]^{-m_w} \tag{6}$$

where a_w, n_w, m_w are model parameters.

A series of constant-water-content triaxial compression tests were carried out on Chiba sand and additional information on the test program is given in Appendix A. The choice of using this data set instead of suction-controlled tests was motivated by the wide range of initial densities and pressures. Furthermore, the accuracy of a water or air controller is typically around 1 kPa, which makes suction-controlled tests very difficult to carry out on unsaturated sand in the funicular regime. These tests were carried out in duplicates at two different strain rates, which allowed a comparison of the volumetric deformation, and to detect any inconsistency in the measurements. The constant-water-content test implies that the mass of water is conserved throughout the entire test and, hence, the degree of saturation and the matric suction were free to change with the volumetric deformation. Toll (1988) and Ng and Menzies (2007) showed that the changes in matric suction in granular material were consistent with the changes in volume for matric suction within the funicular regime. Sand tends to dilate and the degree of saturations decreases throughout most of the test. Therefore, it is reasonable to estimate the matric suction of dilative sands with the drying SWRC. Russell and Khalili (2006) carried out both constant-water-content and suction-controlled triaxial compression tests on Kurnell sand, and showed that both methods gave similar results. Fern et al. (2015) also compared suction-controlled and constant-water-content triaxial compression tests of Chiba sand, and also showed that they gave similar results. The matric suction of the constant-water-content tests was estimated with the SWRC. However, the matric suction in sand is typically lower than 10 kPra and, hence, its contribution to the mean effective stress is limited. Nevertheless, the validity of the effective stress principle is paramount for the stress-dilatancy theory and hence for the analysis.

STRESS-DILATANCY RELATIONSHIP

The results of triaxial tests are commonly presented in two figures, one for the shear strength and one for the volumetric behaviour. However, it is possible to present both behaviours in a single figure in the form of a stress-dilatancy curve. The use of a stress ratio allows a better comparison between tests at different confining pressures. Fig. 2 shows a schematic description of a triaxial compression test. Fig. 2(a) shows the development of the effective stress ratio with dilatancy, Fig. 2(b) the development of strength with deviatoric strains and Fig. 2(c) the volume changes with deviatoric strains. In triaxial compression tests, the specimen first undergoes a short contraction of typically 1% volumetric strain for 1% to 5% deviatoric strain (points A to B). It can be seen that this contraction appears to be more significant in the stress-dilatancy curve due to the low stresses ($\eta' = q/p'$). At point B, the specimen starts dilating and developing a peak strength which is reached at point C. The specimen then softens from point C to B' but is still dilating. It reaches the critical state at point B'.

In order to facilitate the reading, all the figures shown in this paper have the same marker and color convention. The markers correspond to the three different initial densities ($\circ$ loose, $\Box$ medium-dense and $\Diamond$ dense) and the color to their initial water content - black for saturated specimens, and shadings of gray for partially saturated specimens. The void ratio and the degree of saturation used for the analyses were updated throughout the tests with the volumetric strain.

Fig. 3 shows the stress-dilatancy curves of the constant-water-content tests with an axial rate of 0.1%/min. The three top sub-figures (a-c) show the results for the dense specimens, the three middle sub-figures (d-f) for the medium-dense and the three bottom sub-figures (g-i) for the loose specimens. Each series of sub-figures (a-c, d-f & g-i) are, respectively, for three different initial mean net pressures (p_0^{net} = 20, 40 & 80 kPa). Each sub-figure contains two stress-dilatancy curves, respectively, for a water content of 10% and 17%. A trend line has been plotted for each test in order to facilitate the interpretation of results.

The results show an initial contraction ($D > 0$) followed by dilation ($D < 0$). The magnitude of the contraction and dilation phases increased as the initial density increased. The transition point between both phases ($D = 0$) occurred at a stress state which, in some cases, differed from the critical state. The loose and medium-dense specimens (d-i) reached this transition state at an effective stress ratio lower or equal to the critical state value and the dense specimens (a-c) for values equal or slightly higher. It is also common for saturated sand to exhibit a transition point different from the critical state value (Jefferies and Been 2006; Jefferies and Shuttle 2011). Beyond this point, all specimens dilated. The minimum dilatancy rate was reached in the region of the maximum effective stress ratio. The results show that there was an increase in the peak strength and the dilatancy rates with density, but also with partial saturation. Fig. 4(a) shows the peak states (D_{min}, η'_{max}) of all tests in which the influence of partial saturation can clearly be seen. The peak strengths and dilatancy rates evolved simultaneously with density and partial saturation following the same stress-dilatancy slope. This slope defines the dilatancy parameter N in Nova's flow rule (Eq. 1) and was found to be 0.3. Fig. 4(b) shows a schematic description of the observed increases in peak states. The influence of partial saturation on the peak state was more significant for dense specimens than for the loose ones. Specimens softened after reaching the peaks state and headed towards the critical state. The critical state stress ratio ($\eta'_{cs} = M$) was uniquely defined when expressed as effective stresses. However, the contribution of suction on the critical state effective stresses is small, albeit necessary from a theoretical point of view. The results show that, despite tending towards the critical state, dense specimens underwent strain localization. This can be seen in Fig. 3(a-c). The stress-dilatancy curve suddenly goes from a smooth softening slope to a plateau ($\eta' = cst > M$, $D \to 0$). The strain localization in dense specimens prevents them from reaching the critical state. This issue has been discussed for saturated sand in Roscoe (1970) and Desrues et al. (1996). Higo et al. (2011) showed that partial saturation increased the susceptibility of dense specimens to exhibit strain localization. Loose specimens were not sheared sufficiently to reach the critical state, and the final stress state did not reach the nil dilatancy condition.

Despite little research on the behavior of unsaturated sands, there is some experimental evidence of the enhancement of both the peak strength and the dilatancy rates. However, the investigation of the dilatancy characteristics requires a large number of tests in order to capture the contribution of density, pressure and partial saturation, which are rarely available. Schnellmann et al. (2013) carried out suction-controlled direct shear tests on a silica sand called Eschenbach sand,

and the results clearly show an enhancement of the peak strength and dilatancy rates with little changes in the critical state strength. However, the testing program was limited to a single density. Russell (2004) carried out triaxial compression tests on unsaturated Kurnell sand at two different densities but at two different pressures. Additionally, the specimens were largely in the pendular regime. Robert (2010) carried out constant-water-content direct shear tests and suction-controlled triaxial compression tests on Chiba sand and Cornell sand. The direct shear tests clearly showed an enhancement of the dilatancy characteristics with partial saturation. The suction-controlled tests were carried out for one density which limited the investigation of the dilatancy characteristics.

Toll (1988, 1990) suggested that partial saturation caused a modification of the soil fabric which disturbed the way the packets of grains override one another during the development of strength. Ng and Menzies (2007) also believed in a modification of the soil fabric by partial saturation. Scholtès et al. (2009) concluded, on the basis of discrete element modeling, that partial saturation would inevitably result in a different fabric as the formation of new inter-particles bonds would modify the way force are transmitted from one end of the specimen to another. Oda (1972), Tatsuoka (1987) and Lam and Tatsuoka (1988) showed for saturated Toyoura sand that a modification of the soil fabric caused an enhancement of the peak strength and the minimum dilatancy rate. Furthermore, Oda (1972) observed that the stress-dilatancy slope, captured by the dilatancy parameter N in Eq. 1, remained constant. The results suggest that the enhancement of the minimum dilatancy rate is due to a modification of the soil fabric caused by the presence of menisci. From a micro-mechanical point of view, the formation of menisci results in the enhancement of tensile strength and, from a macro-mechanical point of view, the formation of menisci results in an enhancement of the dilatancy characteristics and effective stresses, and therefore of strength. The effective stress alone is insufficient to explain the enhancement of the peak strength.

STATE INDEXES

The prediction of the minimum dilatancy rate can be achieved with state indexes such as the state parameter (Been and Jefferies 1985) or the relative dilatancy index (Bolton 1986). They have been shown to be powerful modeling proxies for dilatancy and are commonly used in constitutive modeling. The state parameter (Eq. 2) is a theoretical state index which was developed from the critical state theory and relies on it to be quantified. Jefferies (1993) suggested estimating the minimum dilatancy rate by converting the state parameter with the dilatancy coefficient X (Eq. 7) introduced by Jefferies and Shuttle (2002). It was later recognized by (Jefferies and Been 2006) that the dilatancy coefficient X would be fabric dependent.

$$D_{min} = X \cdot \psi \tag{7}$$

where ψ is the state parameter, e the void ratio and e_{cs} the critical state void ratio

An alternative to the state parameter is the relative dilatancy index (Eq. 8) which is a better suited index for experimental data as it does not require the establishment of the critical state line.

$$I_R = I_D \cdot I_C - 1 \tag{8}$$

The relative dilatancy index takes into account the contributions of density through the relative density index (Eq. 9), and pressure through the relative pressure index (Eq. 10).

$$I_D = \frac{e_{max} - e}{e_{max} - e_{min}} \tag{9}$$

$$I_C = \ln\left(Q/p'\right) \tag{10}$$

Bolton (1986) suggested using the relative dilatancy index as a proxy for the maximum axial dilatancy rate $D_{1,min}$ by using a dilatancy coefficient α. Tatsuoka (1987) pointed out that this conversion was fabric dependent. The maximum axial dilatancy rate $D_{1,min}$ is fully equivalent to the dilatancy rate D defined in this paper. However, the conversion from the axial dilatancy rate to a dilatancy rate is non-linear. The same applies to the relative dilatancy index and the state parameter despite both indexes being fully equivalent.

$$D_{1,max} = max\left(\frac{d\varepsilon_v}{d\varepsilon_1}\right) = \alpha \cdot I_R \tag{11}$$

where I_R is the relative dilatancy index, I_D the relative density index, I_C the relative pressure index, e_{max}, e_{min} and e are respectively the maximum, minimum and actual void ratios and Q the crushing pressure for which values are given in Bolton (1986).

The relative dilatancy index is believed to be valid for unsaturated sand as its components remain valid. The relative density index is a description of the pore space regardless of the fluids inside and, therefore, should be independent of partial saturation. Both the minimum and the maximum void ratio are considered to be material properties. The crushing pressure is a property of the mineral as discussed in (Bolton 1986). If the effective stress principle is valid for unsaturated sand, the relative dilatancy index should also be valid. However, an increase in effective stresses by partial saturation would result in a lower relative dilatancy index and in dilatancy rate for a given α. An increase in the inter-particle bonding forces, due to the presence of menisci, would prevent some dilatancy as particles are bonded to one another and, hence, the relative dilatancy index is correctly smaller. However, experimental observations (Fig. 4a) show an enhancement of the dilatancy rates which suggests that α would change with partial saturation.

There is an alternative approach to investigate the validity of the relative dilatancy index. Mitchell and Soga (2005) showed that the relative dilatancy index could be converted into a critical state line as the relative dilatancy index are nil at critical state (Eq. 12) and that the critical state density is not influenced by the soil fabric.

$$e_{cs} = e_{max} - \frac{e_{max} - e_{min}}{\ln(Q/p')} \tag{12}$$

This critical state line is non-linear with a sharp change in slope as the pressure increases towards the crushing pressure. Fig. 5(a) shows the critical state line for saturated Toyoura sand from Verdugo and Ishihara (1996). It demonstrates that the relative dilatancy index can predict the critical state void ratio of saturated silica sand. Russell and Khalili (2006) noticed that, unlike for unsaturated clays, the critical state line of Kurnell sand was the same as for saturated and unsaturated sands when stresses were expressed as effective (Fig. 5b).

Fig. 6(a) and (b) show the evolution of void ratio for dry and unsaturated medium-dense Chiba sand, respectively, for an axial strain rate of 0.1%/min and 5.0%/min. The choice of presenting the medium-dense tests was to avoid tests which were not sufficiently sheared or had undergone strain localization. The dry specimens were prepared by dry pluviation and the unsaturated by wet tamping which inferred different fabrics to the soil. However, both the dry and the unsaturated specimens reached the same critical state line. The results suggest that the critical state line is unique for unsaturated Chiba sand and that the relative dilatancy index is valid. The establishment of a critical state for unsaturated sand permits a quantification of the state parameter. This is a major difference with other researchers who used conventional critical state lines to quantify the state parameter.

Fig. 7(a) and (b) show, respectively, the relative dilatancy index and the state parameter for Chiba sand for the different strain rates which offered redundancy in the computed variables. Whilst the relative dilatancy index and the state parameter are still valid for unsaturated sand, the results suggest that their conversion to a dilatancy rate are partial saturation dependent. This is consistent with Tatsuoka (1987) and Jefferies and Been (2006) who suggested a dependency to the soil fabric.

It is common in unsaturated soil mechanics, but not exclusive, to use the matric suction as a model variable. Sands have a very small air entry value, often below 1 kPa (*i.e.* Likos et al. 2010). Therefore, the error committed by neglecting this air entry value is limited. It is then possible to use the degree of saturation S_w as a model variable which allows the model to be formulated over the entire domain of saturation. There is some evidence that the shear strength and dilatancy drops beyond the residual degree of saturation (*i.e.* Donald 1956; Vanapalli et al. 1996; Lu and Likos 2006). Robert (2010) showed this drop in strength for Chiba sand in direct shear tests. Russell and Khalili (2006) showed evidence of loss of strength with increasing suction in suction-controlled oedometer which is consistent with the collapse of a sand castle by drying. By using the degree of saturation as a model variable, it is possible to differentiate the changes in mechanical properties by drying and wetting.

The enhancement of the dilatancy coefficient with partial saturation can be decomposed into a saturated term and a partially saturated term (Eq. 13).

$$X = X_{sat} + \Delta X \cdot f_{(S'_w)} \tag{13}$$

where X_{sat} is the dilatancy coefficient for saturated and dry conditions, ΔX the maximum enhancement value and $f_{(S'_w)}$ the shape function. The enhanced part of the dilatancy coefficient can be formulated as a maximum enhancement ΔX, which would occur at a certain degree of saturation S_w^{max}, and a shape function.

Vanapalli et al. (1996) suggested that the maximum strength enhancement would occur around the residual degree of saturation. Therefore, the degree of saturation at maximum strength would relate to the residual degree of saturation. However, in order to be general and avoid confusion, the degree of saturation at maximum enhancement will be referred to as S_w^{max}. The shape function can be formulated as a function of the effective degree of saturation S'_w and expressed in Eq. 14.

$$f_{(S'_w)} = \frac{\exp\left(-\beta \cdot {S'_w}^2\right) - \exp(-\beta)}{1 - \exp(-\beta)} \tag{14}$$

The effective degree of saturation, has a maximum value of 1 at $S'_w = 0$ and 0 at $S'_w = 1$, can be formulated over the entire domain of saturation as shown in Eq. 15.

$$S'_w = \begin{cases} \dfrac{S_w - S_w^{max}}{1 - S_w^{max}} & \text{if} \quad S_w \geq S_w^{max} \\ \\ \dfrac{S_w^{max} - S_w}{S_w^{max}} & \text{if} \quad S_w < S_w^{max} \end{cases} \tag{15}$$

where f is the shape function, S'_w the effective degree of saturation, $S_w'^{max}$ the degree of saturation at maximum enhancement and β the shape function coefficient.

Fig. 8(a) shows the shape function for different vales of β in which it can be seen that high values of the shape parameter concentrate the enhancement around the nil effective degree of saturation. The shape function is continuously derivable over the entire domain of saturation and for any value of β. This implies that the value of β can differ from the wet and dry side. High values of β minimizes the influence of the neglected air entry value at full saturation. Fig. 8(b) shows the calibration of the shape function for the constant-water-content tests on Chiba sand. The black markers are the mean values obtained from Fig. 7.

CONSTITUTIVE MODELING

The stress-dilatancy rule (Eq. 1) was shown to be valid for both saturated and partially saturated sands which implies that existing constitutive models for saturated sands can be extended to partially saturated conditions. The ability to predict the critical state effective stress ratio M and the dilatancy rates at peak state offers unprecedented convenience in modeling. Jefferies (1993) suggested a model called Nor-Sand which was developed from Nova's stress-dilatancy rule (Eq. 1) by means of normality (Drucker et al. 1957) and, therefore, preserves the shape of the yield function for partially saturated conditions. The Nor-Sand models was made non-associative by Borja and Andrade (2006) and will be used to demonstrate the enhancement by partial saturation of the dilatancy characteristics.

The Nor-Sand model can be viewed as an Original Cam-Clay model (Roscoe and Schofield 1963) with sub-loading surface (Hashiguchi and Chen 1998) for sands and for which the maximum yield surface is determined as a function of the dilatancy characteristics. It assumes that plasticity takes place prior to the peak state. The Nor-Sand model sizes the yield and the potential surfaces with the image pressures which correspond to the pressure at the tip of the surface as shown in Fig. 9. The image pressures are equal to the mean effective stress at critical state ($p' = p_i = p_{i,p}$). Eqs. 16 and 17 give the yield and potential functions, respectively.

$$F = \eta' - \frac{M}{N_f}\left[1 + (N_f - 1)\left(\frac{p'}{p_i}\right)^{\frac{N}{1-N_f}}\right] \quad \text{for} \quad N_f > N_p > 0 \tag{16}$$

$$P = \eta' - \frac{M}{N_p}\left[1 + (N_p - 1)\left(\frac{p'}{p_{i,p}}\right)^{\frac{N_p}{1-N_p}}\right] \quad \text{for} \quad N_f > N_p > 0 \tag{17}$$

where F is the yield function, P the potential function, N_f and N_p the dilatancy parameters for ,respectively, the yield and potential functions, and p_i and $p_{i,p}$ the image pressures for the yield and potential functions, respectively.

The inclusion of a new variable to capture the partial saturation implies that the consistency condition has to be extended (Eq. 18) and the derivatives of the yield and potential functions have to be obtained consequently.

$$dF = \frac{\partial F}{\partial \sigma} d\sigma + \frac{\partial F}{\partial p_i} \frac{\partial p_i}{\partial \varepsilon_d^p} d\varepsilon_d^p + \frac{\partial F}{\partial p_i} \frac{\partial p_i}{\partial S_w} dS_w \tag{18}$$

The Nor-Sand model assumes that the hardening and softening rates are proportional to the distance between the current state, characterized by the image pressure p_i, and the maximum predicted state, characterized by the maximum image pressure $p_{i,max}$. The proportionality between the hardening rate and the difference in image pressures defines the hardening modulus H. The maximum image pressure is estimated by considering the dilatancy characteristics of the soil (Eq. 19).

$$\frac{p_{i,max}}{p'} = \left(1 + D_{min} \cdot \frac{N_f}{M}\right)^{\frac{N_f - 1}{N_f}} \tag{19}$$

where $p_{i,max}$ is the maximum image pressure

The hardening concept is similar to the one expressed for bounding surface models (*i.e.* Russell and Khalili 2006) or subloading surfaces (*e.g.* Hashiguchi and Chen 1998). The hardening rule can be expressed as shown in Eq. 20.

$$\frac{\dot{p}_i}{\dot{\varepsilon}_d^p} = H \cdot M \exp\left(1 - \frac{\eta'}{M}\right) \cdot (p_{i,max} - p_i) \tag{20}$$

where $H = H_{min} \exp(\delta_H I_D)$ is the hardening modulus, which is dependent on the state parameter (Jefferies and Been 2006), and H_{min} is the minimum hardening modulus for very loose sand and δ_H its enhancement by density.

The prediction of minimum dilatancy rate (Eq. 21) was updated due to the non-associativity

(Borja and Andrade 2006) and for which the dilatancy parameter N_p is obtained from the stress-dilatancy curves (Fig. 4).

$$D_{min} = \chi \cdot \frac{1 - N_p}{1 - N_f} \cdot \psi_i \tag{21}$$

Partial saturation enhances the mean effective stress and the dilatancy characteristics which then enhance the maximum image pressure $p_{i,max}$. It results in a higher peak strength as well as an enhancement of the hardening and softening rates which infer additional brittleness to the material and a higher susceptibility to strain localization.

The Nor-Sand model considers the tangent elastic properties which are those of an unloading-reloading cycle. It is widely accepted that the shear modulus G increases with pressure (Eq. 22).

$$G = A \left(\frac{p'}{p_{ref}} \right)^n \tag{22}$$

Alonso et al. (2010) suggested a similar expression in which the enhancement of the elastic properties is solely captured by the enhancement of the effective stress. The bulk modulus K may then be deduced from the shear modulus (Eq. 23). The Poisson ratio is assumed to be constant.

$$K = \frac{2(1+\nu)}{3(1-2\nu)} \cdot G \tag{23}$$

where G is the shear modulus, A is the shear modulus constant, n the shear modulus exponent, p_{ref} the unit reference pressure, K the bulk modulus and ν the Poisson ratio.

Simulating triaxial compression tests

The calibration of the model parameters is obtained from laboratory tests with the exception of the hardening modulus H and the dilatancy parameter of the yield function N_f. The values of the model parameter are summarized in Table 2. The elastic parameters (A, n, p_{ref}) have been calibrated on an unloading and reloading cycle and the Poisson ratio ν was taken as a constant. The critical state effective stress ratio M and the dilatancy coefficient for the potential function N_p were obtained from the stress-dilatancy curves. The dilatancy coefficient for the yield surface N_f

was progressively reduced from $N_f = N_p$ until matching the experimental data. The minimum and maximum void ratios e_{min} and e_{max} were obtained by laboratory testing. The crushing pressure Q is given in Bolton (1986). The minimum hardening modulus H_{min} and its coefficient δ_H were obtained empirically. The saturated dilatancy coefficient X_{sat}, its maximum enhancement ΔX and the shape function coefficient β_{wet} were obtained from the dilatancy analysis. The shape function parameter β_{dry} was set at 0.5 arbitrarily as no data was available and no simulations will be carried out in that region of saturation.

The triaxial compression tests, presented in Fig. 3, were simulated using a single-element code and the results are presented in Fig. 10 and 11. The simulations of the dense specimens (Fig. 10a-b and 11a-b) are in agreement with the experimental data. The hardening phase, the peak strength and the minimum dilatancy rate are well captured by the model. However, some differences emerge between the simulations and the experimental data in the softening phase. This is largely because of strain localization, which is accentuated by the enhancement of the dilatancy characterized, and cannot be captured by single-element simulations. However, the Nor-Sand model is capable of capturing the formation of shear bands as it was demonstrated by Andrade (2006).

The simulations of the medium-dense specimens (Fig. 10c-d and 11c-d) are in better agreement with the experimental data due to the absence of strain localization. The hardening phase, the peak strength and the minimum dilatancy rate were well captured by the model as well as the softening phase due to the absence of strain localization. The specimens, therefore, underwent a homogeneous failure which is in accordance with the stress-dilatancy and critical state theories.

The simulations of the loose specimens (Fig. 10e-f and 11e-f) are in good agreement with the experimental data. Both the simulations and the experimental data show small dilatancy rates and, hence, peak strengths. Furthermore, the stiffness in the hardening phase is reduced. However, loose specimens have initial void ratios close to the critical state line and, therefore, small errors in the estimation of the initial void ratio as well as small errors in the modeling of the critical state line lead to errors in the estimation of the dilatancy rate. The mechanical behavior of loose sand is sensitive to its initials density. This issue has been pointed out by Jefferies and Been (2006) who highlighted the importance of obtaining accurate initial void ratios. This sensitivity is increased at low pressures where dilatancy is more significant.

The overall results of the simulations are very consistent with the experimental data and this over a wide range of densities and for three different pressures. Unlike classical elastic-plastic models, the presented model is able to capture the correct peak strength and dilatancy rates of partially saturated sand and this with only four additional parameters.

Simulating wetting-collapses

The collapse of soil upon wetting is a major concern in terms of understanding and modeling of unsaturated soil. Leonards (1962) suggested that the collapse was due to a rearrangement of the grains resulting in a smaller packing and, therefore, a loss of dilatancy characteristics. Alonso et al. (1990) succeeded in modeling the wetting-collapse by introducing the loading-collapse (LC) curve which assumes that the on-set of collapse was a yielding point. However, as Russell and Khalili (2006) and Masin and Khalili (2008) demonstrated, the inclusion the loading-collapse is only a necessity for models which consider the peak state as a yielding point.

Fig. 12 shows a triaxial compression tests in which wetting was undertaken at an axial strain of 4% (point B). As wetting took place, the dilatancy characteristics and the mean effective stress, albeit more limited, decreased which caused a decrease of the maximum image pressure and, hence, the peak state. From point B to C, the maximum image pressure was larger than the image pressure and the model predicted some swelling. The hardening rule (Eq. 20) was positive. From point C to D, the maximum image pressure was smaller than the image pressure and the model predicted a collapse. The hardening rule (Eq. 20) was negative. Fig. 13 illustrates both behaviors. The continuous line corresponds to the yield surface defined by the current image pressure. The dashed line corresponds to the peak state yield surface defined by the maximum image pressure.

The ability of the model to capture both the enhancement of the peak strength and the wetting behaviors is not a coincidence. The size of the maximum yield surface is controlled by the dilatancy characteristics. When the soil is wetted, the loss of dilatancy caused the maximum yield surface to shrink. Therefore, the predicted peak strength is lower. If the maximum yield surface shrinks sufficiently to be smaller than the current yield surface, a collapse will occur. The large collapse shown in Fig. 12 is due to the large loss of dilatancy characteristics of Chiba sand. Sands with smaller dilatancy characteristics would result in smaller collapses.

CONCLUSIONS

The investigation of the stress-dilatancy relationship of an unsaturated silica sand showed that the stress-dilatancy theory was still valid. The increase in peak strength was found to be solely a consequence of an increase of the dilatancy characteristics. These increases are consistent with a modification of the soil fabric. The formation of menisci at inter-particle contact which change the way packets of grains override one another. The modification of the dilatancy characteristics also explains the changes in the hardening and softening rates and, hence, the higher susceptibility of partially saturated dense sand to undergo strain localization (Higo et al. 2011).

The use of state indexes as proxies for dilatancy were also found to be valid. However, the modification of the soil fabric by partial saturation lead to an enhancement of the dilatancy coefficients. This is consistent with observation made for saturated sands. However, it can be argued, from a micro-mechanical point of view, that the conversion of a state index to a dilatancy rate cannot be captured by a scalar (*e.g.* Li and Dafalias 2012) and additional investigations should be undertaken.

The validity of the stress-dilatancy rule for unsaturated sand and the ability to predict the peak state offers unprecedented ease in modeling the mechanical behavior of unsaturated sand. This was demonstrated with the Nor-Sand model (Jefferies 1993; Borja and Andrade 2006) for which only four additional parameters were required to capture the increase in shear strength and dilatancy rates as well as the swelling and collapse by wetting. The proposed modification to the Nor-Sand model is not unlike the one proposed by Alonso et al. (1990) for the Cam-Clay model but is applied to the maximum image pressure instead of the preconsolidation pressure and is included the density as a model variable.

ACKNOWLEDGEMENT

The authors would like to thank Dr Takashi Sakanoue from Tokyo Gas, Japan, for his technical and financial support. This project has received funding from the European Unions Seventh Framework Program for research, technological development and demonstration under grant agreement no PIAP-GA-2012-324522 and from the Swiss National Science Foundation under grant agreement P1SKP2 158621.

APPENDIX A - TRIAXIAL COMPRESSION TEST PROGRAM

The specimens for the triaxial tests were prepared to achieve a specific density and water content. The specimens were then prepared by wet tamping and shaped into 100 mm x 50 mm cylinders. The tamping protocol was strictly followed for each specimen in order to obtain repeatable test. The specimens were consolidated to a specific net pressure. The pressure were chosen to be low in order to favor the dilative behavior of Chiba sand.

The constant-water-content tests were carried out as 'undrained' in the sense the mass of water was conserved throughout the test in a similar way Russell (2004) did for Kurnell sand. The volume change was monitored with the cell water and care was taken to avoid any entrapment of air in the cell volume which would lead to errors in the assessment of the volumetric strain increments used to compute the dilatancy rates and the degrees of saturation. The pressure was kept constant during the entire shearing process. The peak state, which is of concern, was reached in less than 15 minutes for the longest test and around 3 minutes for the shortest. Therefore, secondary deformation of the cell casing can be neglected. Furthermore, the tests carried out at 0.1%/min and 5.0%/min were exact duplicates and showed consistent changes in volume. Tables 3 and 4 give the initial state after consolidation.

The matric suctions were estimated from the degree of saturation using the water retention curves (Fig. 1b). These curves were obtained on the drying path which is consistent with dilative sand. The influence of the hysteresis on the effective stress is expected to be significantly lower than the influence of strain localization on the critical state strength. The suction of sand is very low and the suction-induced effective stress less than 10 kPa.

NOTATION

The following symbols are used in this paper:

a = micro-structure exponent;

A = shear modulus constant;

D = dilatancy rate;

D_{min} = minimum dilatancy rate;

$D_{1,max}$ = maximum axial dilatancy rate;

d = grain size;

e = void ratio;

e_{cs} = critical state void ratio;

e_{max} = maximum state void ratio;

e_{min} = minimum void ratio;

f = shape function;

F = yield function;

P = potential function;

G = shear modulus;

H = hardening modulus;

H_{min} = minimum hardening modulus;

I_C = relative pressure index;

I_D = relative density index;

I_R = relative dilatancy index;

K = bulk modulus;

M = critical state stress ratio;

m_w = van Genuchten model parameter;

N = dilatancy parameter;

N_f = dilatancy parameter for yield function;

N_p = dilatancy parameter for potential function;

n = shear modulus exponent;

n_w = van Genuchten model parameter;

p_a = pore air pressure;

p_w = pore water pressure;

p' = mean effective stress;

p'_{cs} = critical state mean effective stress;

p'_{max} = maximum mean effective stress;

p'_i = image pressure of yield function;

$p'_{i,p}$ = image pressure of potential function;

$p'_{i,max}$ = maximum image pressure;

p'_{ref} = reference unit pressure;

p^{net} = mean net stress;

p^{tot} = mean total pressure;

q = deviatoric stress;

q_{cs} = critical state deviatoric stress;

Q = crushing pressure;

s = matric suction;

s_e = air entry matric suction;

S_{res} = residual degree of saturation;

S_w = degree of saturation;

S'_w = effective degree of saturation;

S_w^{max} = maximum strength degree of saturation;

α = dilatancy coefficient;

α_w = van Genuchten model parameter;

β = shape function coefficient;

δ_H = hardening modulus coefficient;

ΔX = dilatancy coefficient enhancement;

ε_1 = axial strain;

ε_d = deviatoric strain;

ε_d^p = plastic deviatoric strain;

ε_v = volumetric strain;

ε_v^p = plastic volumetric strain;

η' = effective stress ratio;

η'_{max} = maximum effective stress ratio;

X = dilatancy coefficient;

X_{sat} = saturated dilatancy coefficient;

χ = Bishop's coupling parameter;

ψ = state parameter;

ν = Poisson ratio;

REFERENCES

Aitchison, G. D. (1960). "Relationships of moisture stress and effective stress functions in unsaturated soils." *Conf. Pore Pressures and Suction in Soils*, London, Butterworths.

Alonso, E., Gens, A., and Josa, A. (1990). "A constitutive model for partially saturated soils." *Géotechnique*, 40(3), 405–430.

Alonso, E., Pereira, J.-M., Vaunat, J., and Olivella, S. (2010). "A microstructurally based effective stress for unsaturated soils." *Géotechnique*, 60(12), 913–925.

Andrade, J. (2006). "Meso-scale finite element simulation of deformation banding in fluid-aturated sands." Ph.D. thesis, Stanford University, Stanford University.

Bardet, J. P. (1986). "Bounading Surface Plasticity Model for Sand." *Journal of Engineering Mechanics*, 112(11), 1198–1217.

Been, K. and Jefferies, M. G. (1985). "A state parameter for sands." *Géotechnique*, 35(2), 99–112.

Bishop, A. (1959). "The principles of effective stress." *Tecnisk Ukeblad*, 8, 859–863.

Bishop, A. and Blight, G. (1963). "Some Aspects of Effective Stress in Saturated and Partly Saturated Soils." *Géotechnique*, 13(3), 177–197.

Bolton, M. (1986). "The strength and dilatancy of sands." *Géotechnique*, 36(1), 65–78.

Bolzon, G., Schrefler, B. A., and Zienkiewicz, O. C. (1996). “Elastoplastic soil constitutive laws generalized to partially saturated states.” *Géotechnique*, 46(2), 279–289.

Borja, R. I. and Andrade, J. E. (2006). “Critical state plasticity. Part VI: Meso-scale finite element simulation of strain localization in discrete granular materials.” *Computer Methods in Applied Mechanics and Engineering*, 195(37-40), 5115–5140.

Chiu, C. F. and Ng, C. (2003). “A state-dependent elasto-plastic model for saturated and unsaturated soils.” *Géotechnique*, 53(9), 809–829.

Coleman, J. D. (1962). “Stress-strain relations for partly saturated soil.” *Géotechnique*, 12(4), 348–350.

Cui, Y. and Delage, P. (1996). “Yielding and plastic behaviour of an unsaturated compacted silt.” *Géotechnique*, 46(2), 291–311.

Dafalias, Y. F. and Popov, E. P. (1975). “A model of nonlinearly hardening materials for complex loading.” *Acta Mechanica*, 21(3), 173–192.

Desrues, J., Chambon, R., Mokni, M., and Mazerolle, F. (1996). “Void ratio evolution inside shear bands in triaxial sand specimens studied by computed tomography.” *Géotechnique*, 46(3), 529–546.

Donald, I. B. (1956). “Shear Strenght Measurements.” *2nd Australian-New Zeland Conference on Soil Mechanics and Foundation Engineering*, Christchurch, The New Zealand Institution of Engineers, 200–204.

D’Onza, F., Gallipoli, D., Wheeler, S., Casini, F., Vaunat, J., Khalili, N., Laloui, L., Mancuso, C., Masin, D., Nuth, M., Pereira, J. M., and Vassallo, R. (2011). “Benchmark of constitutive models for unsaturated soils.” *Géotechnique*, 61(4), 283–302.

Drucker, D., Gibson, R., and Henkel, D. (1957). “Soil mechanics and work-hardening theories of plasticity.” *Journal of Soil Mechanics and Foundation Engineering1*, 122, 338–346.

Fern, J., Robert, D., Sakanoue, T., and Soga, K. (2015). “Shear Strength and Dilatancy of Unsaturated Silica Sand in Triaxial Compression Tests.” *Computer Methods and Recent Advances in Geomechanics*, F. Oka, A. Murakami, R. Uzuoka, and S. Kimoto, eds., London, Taylor &

Francis, 535–540.

Fredlund, D. G., Morgenstern, N. R., and Widger, R. A. (1978). "The shear strength of unsaturated soils." *Canadian Geotechnical Journal*, 15(3), 313–321.

Geiser, F. (1999). "Comportement mécanique d'un limon non saturé : étude expérimentale et modélisation constitutive." Ph.D. thesis, Ecole Polytechnique fédérale de Lausanne, Ecole Polytechnique fédérale de Lausanne.

Hashiguchi, K. and Chen, Z. P. (1998). "Elastoplastic Constitutive Equation of Soils With the Subloading Surface." *International Journal*, 22(June 1996), 197–227.

Higo, Y., Oka, F., Kimoto, S., Sanagawa, T., and Matsushima, Y. (2011). "Study of Strain Localization and Microstructural Changes in Partially Saturated Sand During Triaxial Tests Using Microfocus X-Ray CT." *Soils and foundations*, 51(1), 95–111.

Jefferies, M. (1993). "Nor-Sand : a simple critical state model for sand." *Géotechnique*, 43(1), 91–103.

Jefferies, M. and Been, K. (2006). *Soil Liquefaction A Critical State Approach*. Taylor & Francis, London.

Jefferies, M. and Shuttle, D. (2002). "Dilatancy in general Cambridge-type models." *Géotechnique*, 52(9), 625–638.

Jefferies, M. and Shuttle, D. (2011). "On the operating critical friction ratio in general stress states." *Géotechnique*, 61(8), 709–713.

Jennings, J. and Burland, J. (1962). "Limitations to the Use of Effective Stresses in Partly Saturated Soils." *Géotechnique*, 12(2), 125–144.

Khalili, N., Geiser, F., and Blight, G. (2004). "Effective Stress in Unsaturated Soils: Review with New Evidence." *International Journal of Geomechanics*, 4(2), 115–126.

Khalili, N. and Khabbaz, M. H. (1998). "A unique relationship for χ for the determination of the shear strength of unsaturated soils." *Géotechnique*, 48(5), 681–687.

Lam, W. and Tatsuoka, F. (1988). "Effects of initial anisotropic fabric and .SIGMA.2 on strength and deformation characteristics of sand.." *Soils and Foundations*, 28(1), 89–106.

Leonards, G. (1962). “Discussion of Jennings and Burland ’Limitations to the use of effective stress in partly saturated soils’.” *Géotechnique*, 12(4), 354–355.

Li, X. and Dafalias, Y. (2012). “Anisotropic Critical State Theory: Role of Fabric.” *Journal of Engineering Mechanics*, 138(3), 263–275.

Likos, W. J., Wayllace, A., Godt, J., and Lu, N. (2010). “Modified direct shear apparatus for unsaturated sands at low suction and stress.” *Geotechnical Testing Journal*, 33(4), 1–13.

Loret, B. and Khalili, N. (2000). “A three-phase model for unsaturated soils.” *International Journal for Numerical and Analytical Methods in Geomechanics*, 24(March 1999), 893–927.

Lu, N. and Likos, W. J. (2004). *Unsaturated Soil Mechanics*. John Wiley & Sons, Hoboken.

Lu, N. and Likos, W. J. (2006). “Suction Stress Characteristic Curve for Unsaturated Soil.” *Journal of Geotechnical and Geoenvironmental Engineering*, 132(2), 131–142.

Maatouk, A., Leroueil, S., and La Rochelle, P. (1995). “Yielding and critical state of a collapsible unsaturated silty soil.” *Géotechnique*, 45(3), 465–477.

Masin, D. and Khalili, N. (2008). “A hypoplastic model for mechanical response of unsaturated soils.” *International Journal for Numerical and Analytical Methods in Geomechanics*, 32(15), 1903–1926.

Mitchell, J. and Soga, K. (2005). *Fundamentals of Soil Behavior*. John Wiley & Sons, Hoboken, 3rd edition.

Ng, C. and Menzies, B. (2007). *Advanced unsaturated soil mechanics and engineering*. Taylor & Francis, New York.

Nova, R. (1982). “A constitutive model for soil under monotonic and cyclic loading.” *Soil mechanics - transient and cyclic loading*, G. N. Pande and C. Zienkiewicz, eds., Chichester, Wiley, 343–373.

Nuth, M. (2009). “Constitutive Modelling of Unsaturated Soils with Hydro-Geomechanical Couplings.” *Report no.*, Ecole Polytechnique Fédérale de Lausanne.

Oda, M. (1972). “The Mechanism of Fabric Changes during Compressional deformation of sand.” *Soils and Foundations*, 12(2), 1–18.

Rampino, C., Mancuso, C., and Vinale, F. (2000). "Experimental behaviour and modelling of an unsaturated compacted soil." *Canadian Geotechnical Journal*, 37(4), 748–763.

Robert, D. (2010). "Soil-Pipeline Interaction in Unsaturated Soils." Ph.d. dissertation, University of Cambridge, University of Cambridge.

Roscoe, K. H. (1970). "The Influence of Strains in Soil Mechanics." *Géotechnique*, 20(2), 129–170.

Roscoe, K. H. and Burland, J. B. (1968). "On the generalised stress-strain behaviour of 'wet' clay." *Engineering plasticity*, J. Heyman and F. Leckie, eds., Cambridge, Cambridge University Press, 535–609.

Roscoe, K. H. and Schofield, A. (1963). "Mechanical behaviour of an idealised wet clay." *2nd European Conference on Soil Mechanics and Foundation Engineering*, Wiesbaden, 47–54.

Roscoe, K. H., Schofield, A., and Wroth, C. P. (1958). "On The Yielding of Soils." *Géotechnique*, 8(1), 22–53.

Russell, A. (2004). "Cavity Expansion in Unsaturated Soils." Ph.D. thesis, University of New South Wales, University of New South Wales.

Russell, A. and Khalili, N. (2006). "A unified bounding surface plasticity model for unsaturated soils." *International Journal for Numerical and Analytical Methods in Geomechanics*, 30(3), 181–212.

Schnellmann, R., Rahardjo, H., and Schneider, H. R. (2013). "Unsaturated shear strength of a silty sand." *Engineering Geology*, 162, 88–96.

Scholtès, L., Hicher, P.-Y., Nicot, F., Chareyre, B., and Darve, F. (2009). "On the capillary stress tensor in wet granular materials." *International Journal for Numerical and Analytical Methods in Geomechanics*, 33(10), 1289–1313.

Stroud, M. (1971). "The behaviour of sand at low stress levels in the simple-shear apparatus." Ph.D. thesis, University of Cambridge, University of Cambridge.

Tatsuoka, F. (1987). "Discussion: The strength and dilatancy of sands." *Géotechnique*, 37(2), 219–226.

Taylor, D. (1948). *Fundamentals of soil mechanics*. Wiley, New York.

Toll, D. (1988). “The behaviour of unsaturated compacted naturally occuring gravel.” Ph.D. thesis, University of London, University of London.

Toll, D. (1990). “A framework for unsaturated soil behaviour.” *Géotechnique*, 40(1), 31–44.

Toll, D. and Ong, B. (2003). “Critical-state parameters for an unsaturated residual sandy clay.” *Géotechnique*, 53(1), 93–103.

van Genuchten, M. (1980). “A closed form equation for predicting the hydraulic conductivity of unsaturated soils.” *Soil Science Society American Journal*, 44, 892–898.

Vanapalli, S., Fredlund, D. G., Pufahl, D., and Clifton, A. (1996). “Model for the Prediction of Shear Strength with Respect to Soil Suction.” *Canadian Geotechnical Journal*, 33, 379–392.

Verdugo, R. and Ishihara, K. (1996). “The Steady State of Sandy Soils.” *Soils and Foundations*, 36(2), 81–91.

Wheeler, S. J. and Sivakumar, V. (1995). “An elasto-plastic critical state framework for unsaturated soil.” *Géotechnique*, 45(1), 35–53.

List of Tables

TABLE 1. van Genuchten (1980) SWRC parameters for Chiba sand

e	S_{res}	α_w	n_w	m_w
[-]	[-]	[kPa^{-1}]	[-]	[-]
0.963	20%	0.50	3.0	0.3
0.815	22%	0.38	3.0	0.3
0.699	24%	0.22	3.2	0.3

TABLE 2. Unsaturated Nor-Sand parameters for Chiba sand.

Label	Symbol	Value
Shear modulus constant	A	2500 kPa
Shear modulus exponent	n	0.5
Reference pressure	p_{ref}	1 kPa
Critical state effective stress ratio	M	1.33
Maximum void ratio	e_{max}	0.946
Minimum void ratio	e_{min}	0.500
Crushing pressure	Q	10 MPa
Dilatancy parameter for yield function	N_f	0.35
parameter for potential function	N_p	0.3
Minimum hardening modulus	H_{min}	160
Hardening modulus coefficient	δ_H	2
Saturated dilatancy coefficient	X_{sat}	2.5
Maximum dilatancy coefficient enhancement	ΔX	3.1
Shape function coefficient on dry side	β_{dry}	0.5
Shape function coefficient on wet side	β_{wet}	3.0
Degree of saturation at maximum enhancement	S_w^{max}	21%

TABLE 3. Initial conditions for long duration triaxial compression tests

Group	w	e_0	$S_{w,0}$	p_0^{net}	$d\varepsilon_1$	$I_{D,0}$	$I_{R,0}$	ψ_0
	[-]	[-]	[-]	[kPa]	[%/min]	[-]	[-]	[-]
Loose	10%	0.842	32%	20	0.1	23%	0.09	-0.01
	10%	0.818	33%	40	0.1	29%	0.47	-0.04
	10%	0.808	34%	80	0.1	30%	0.43	-0.04
	17%	0.845	55%	20	0.1	23%	0.06	-0.01
	17%	0.830	56%	40	0.1	26%	0.28	-0.03
	17%	0.820	56%	80	0.1	28%	0.29	-0.03
Med.-Dense	10%	0.742	37%	20	0.1	46%	1.63	-0.13
	10%	0.738	37%	40	0.1	47%	1.46	-0.12
	10%	0.725	38%	80	0.1	50%	1.34	-0.13
	10%	0.739	37%	40	0.5	46%	1.44	-0.12
	17%	0.745	62%	20	0.1	45%	1.58	-0.12
	17%	0.734	63%	40	0.1	48%	1.52	-0.13
	17%	0.719	64%	80	0.1	51%	1.41	-0.13
	17%	0.734	63%	40	0.5	47%	1.51	-0.13
	27%	0.739	100%	40	0.5	46%	1.44	-0.12
Dense	17%	0.656	41%	20	0.1	65%	2.93	-0.22
	17%	0.659	41%	40	0.1	64%	2.49	-0.20
	17%	0.653	42%	80	0.1	66%	2.14	-0.20
	17%	0.657	70%	20	0.1	65%	2.91	-0.22
	17%	0.648	71%	40	0.1	67%	2.63	-0.22
	17%	0.641	72%	80	0.1	68%	2.28	-0.21

TABLE 4. Initial conditions for short duration triaxial compression tests

Group	w	e_0	$S_{w,0}$	p_0^{net}	$d\varepsilon_1$	$I_{D,0}$	$I_{R,0}$	ψ_0
	[-]	[-]	[-]	[kPa]	[%/min]	[-]	[-]	[-]
Loose	10%	0.838	32%	20	5.0	24%	0.38	-0.03
	10%	0.832	33%	40	5.0	26%	0.34	-0.03
	10%	0.823	33%	80	5.0	28%	0.29	-0.03
	17%	0.834	55%	20	5.0	25%	0.53	-0.04
	17%	0.829	56%	40	5.0	26%	0.43	-0.04
	17%	0.816	57%	80	5.0	29%	0.40	-0.04
Med.-Dense	10%	0.741	37%	20	5.0	46%	1.50	-0.12
	10%	0.737	37%	40	5.0	47%	1.37	-0.12
	10%	0.725	38%	80	5.0	50%	1.27	-0.12
	17%	0.742	62%	20	5.0	46%	1.75	-0.13
	17%	0.732	63%	40	5.0	48%	1.60	-0.13
	17%	0.715	65%	80	5.0	52%	1.48	-0.14
Dense	10%	0.655	42%	20	5.0	65%	2.68	-0.21
	10%	0.649	42%	40	5.0	67%	2.46	-0.21
	10%	0.645	42%	80	5.0	67%	2.14	-0.21
	17%	0.656	70%	20	5.0	65%	2.95	-0.22
	17%	0.647	71%	40	5.0	67%	2.66	-0.22
	17%	0.639	72%	80	5.0	69%	2.30	-0.21

List of Figures

Figure1

Click here to download Figure Fig1.pdf

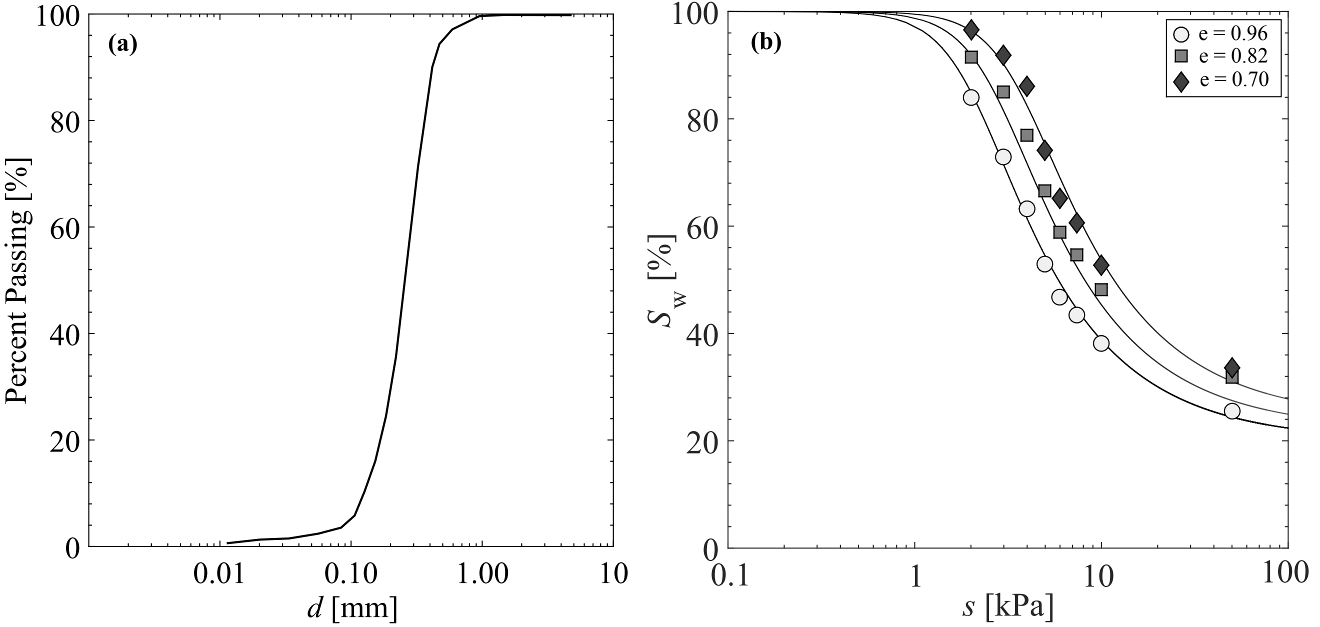

Figure2

Click here to download Figure Fig2.pdf

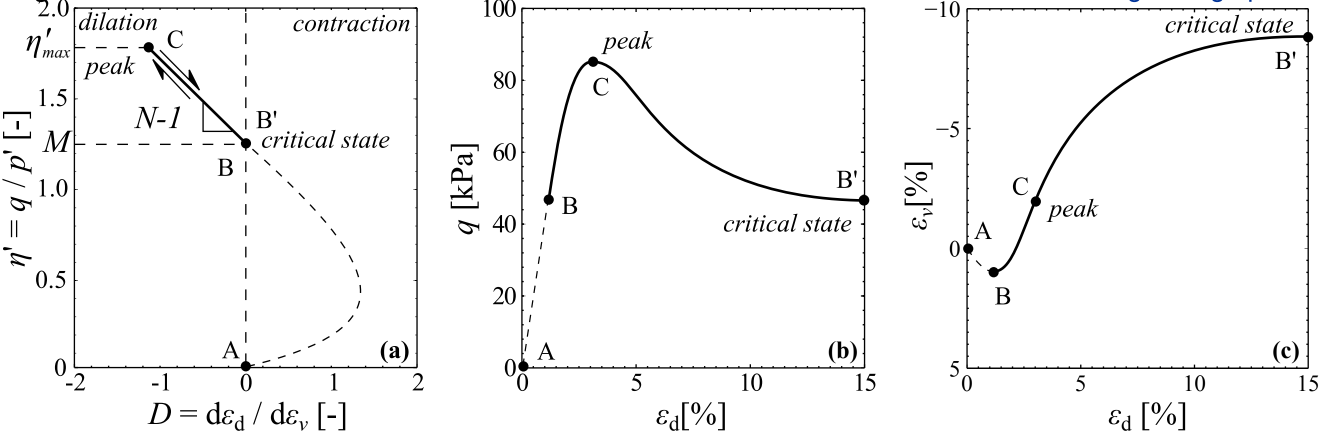

Figure3

Click here to download Figure Fig3.pdf

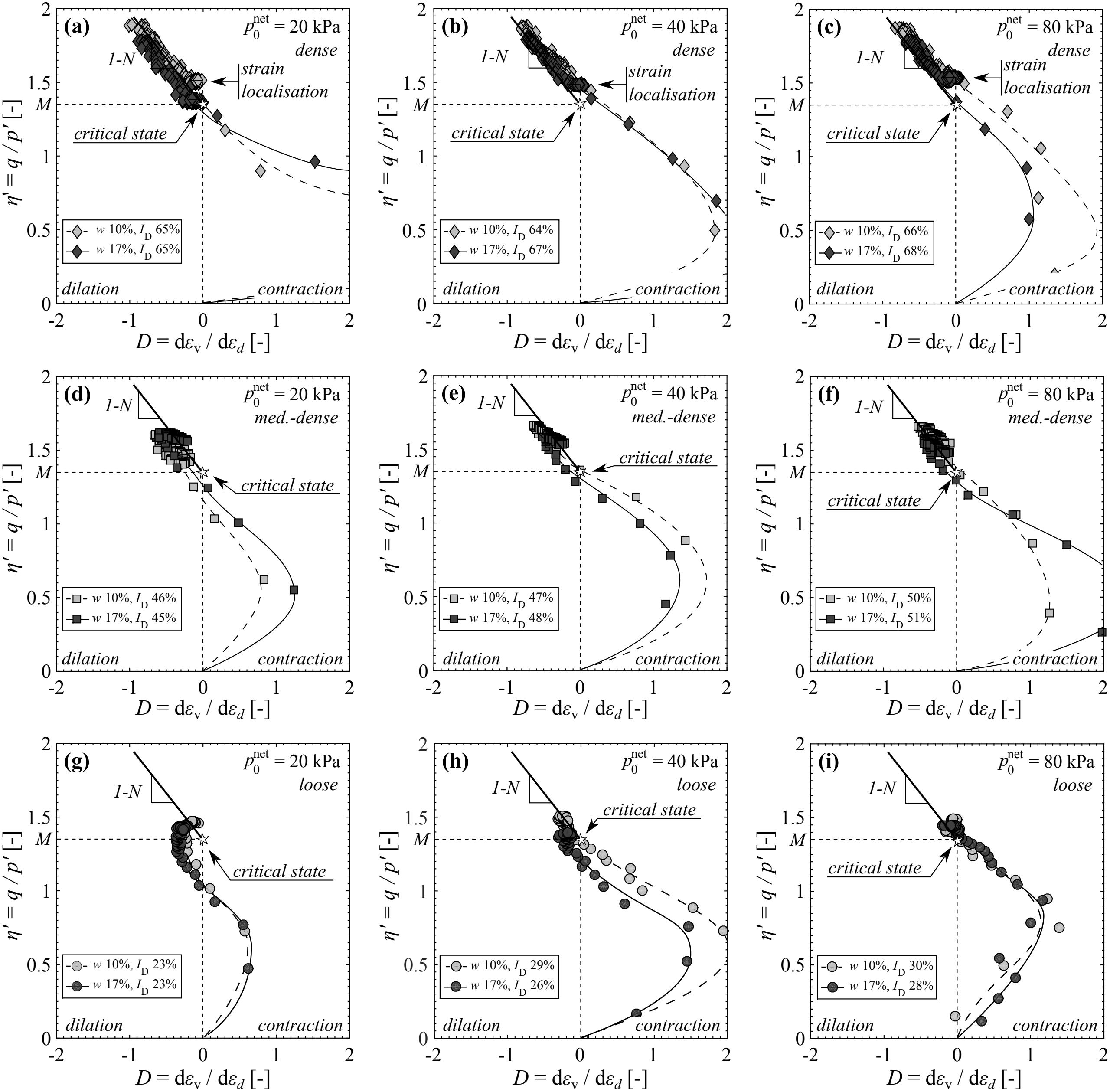

Figure4

Click here to download Figure Fig4.pdf

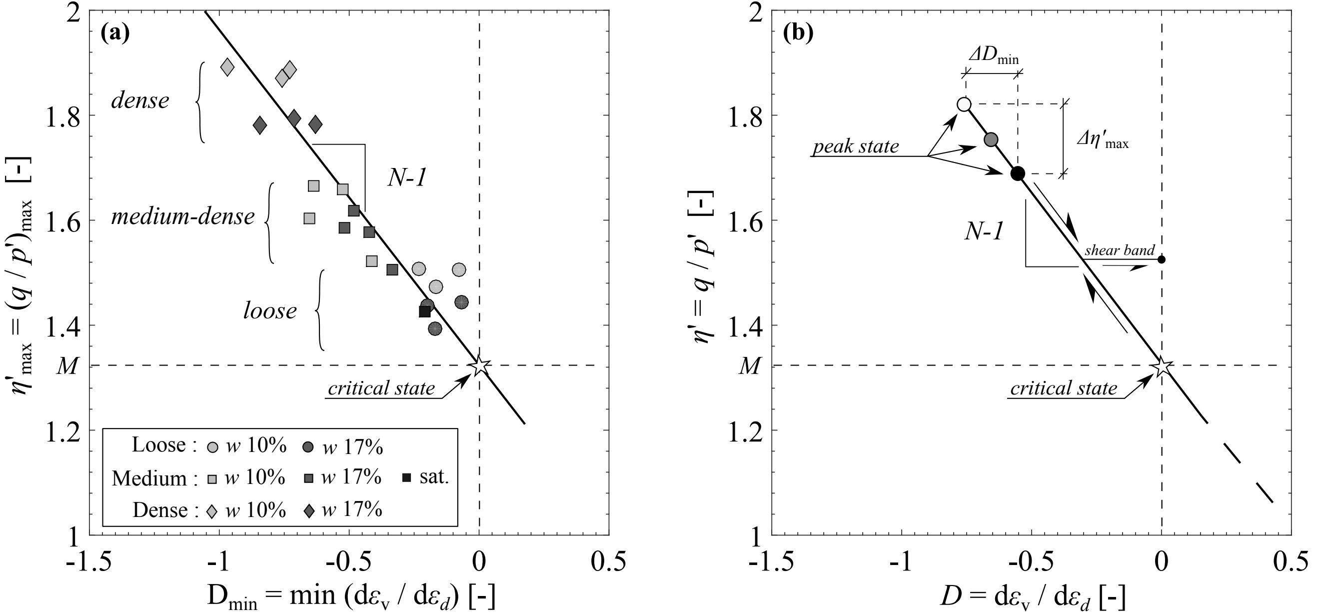

Figure5

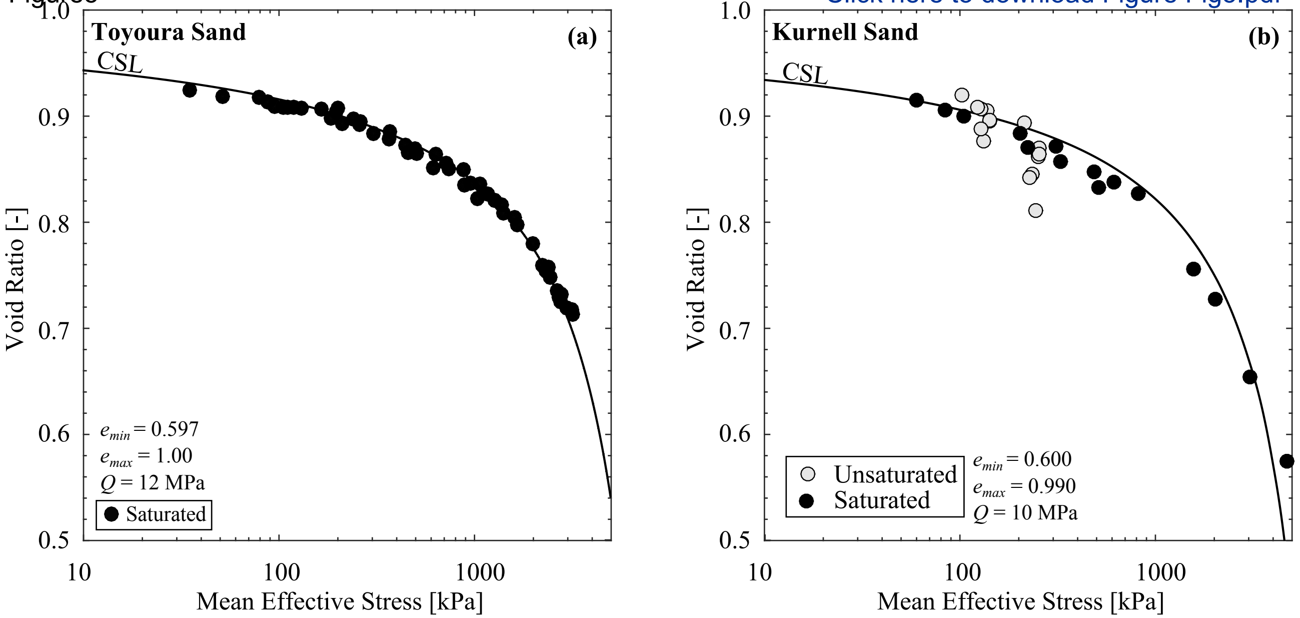
Toyoura Sand
(a)
CSL
e_{min} = 0.597
e_{max} = 1.00
Q = 12 MPa
Saturated
Void Ratio [-]
Mean Effective Stress [kPa]
1.0
0.9
0.8
0.7
0.6
0.5
10
100
1000
Kurnell Sand
(b)
CSL
Unsaturated
Saturated
e_{min} = 0.600
e_{max} = 0.990
Q = 10 MPa
Void Ratio [-]
Mean Effective Stress [kPa]

Figure6

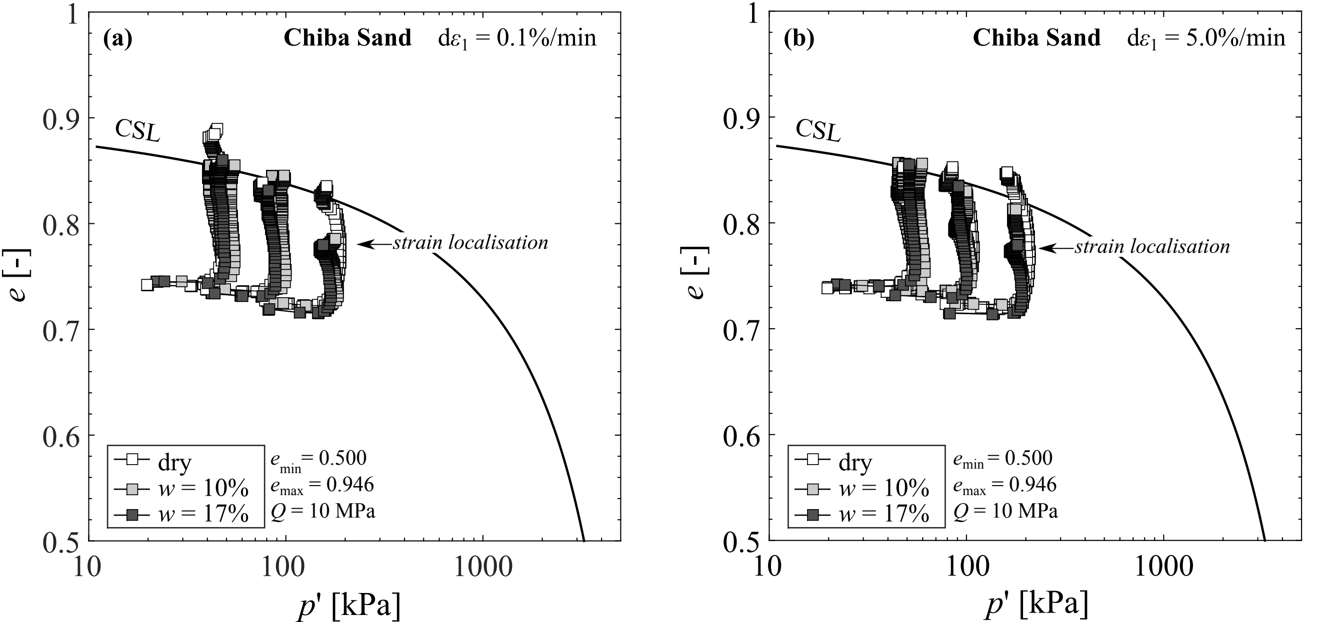

(a)
Chiba Sand
dε1 = 0.1%/min
CSL
strain localisation
dry
w = 10%
w = 17%
emin = 0.500
emax = 0.946
Q = 10 MPa
e [-]
p' [kPa]
1
0.9
0.8
0.7
0.6
0.5
10
100
1000
(b)
Chiba Sand
dε1 = 5.0%/min
CSL
strain localisation
dry
w = 10%
w = 17%
emin = 0.500
emax = 0.946
Q = 10 MPa
e [-]
p' [kPa]

Figure7

Click here to download Figure Fig7.pdf

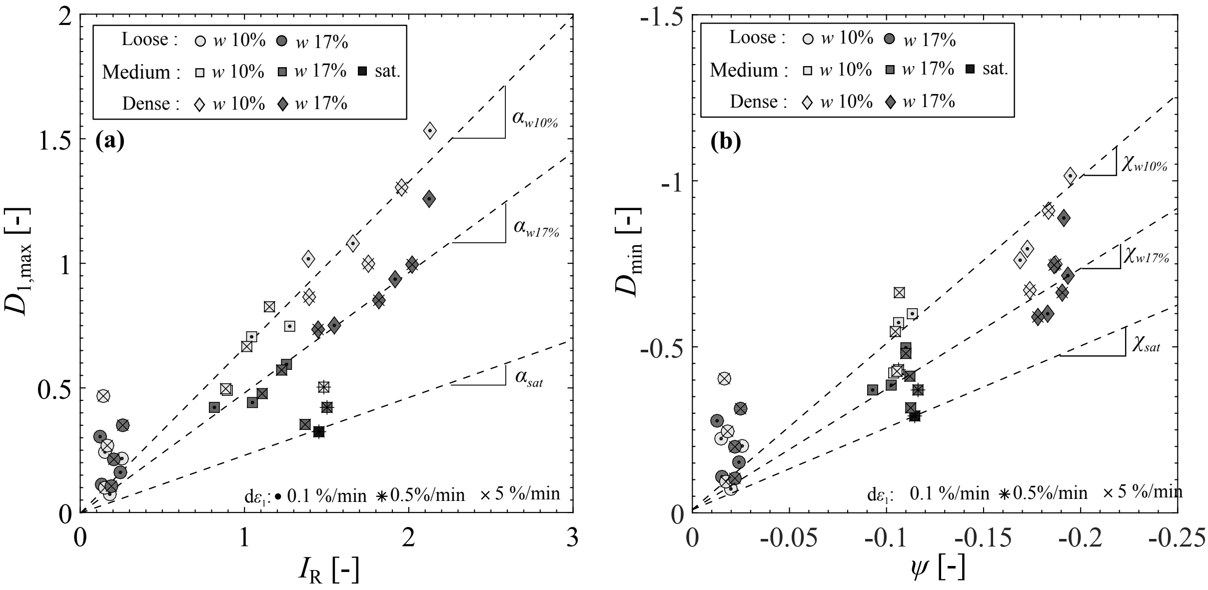

Figure8

Click here to download Figure Fig8.pdf

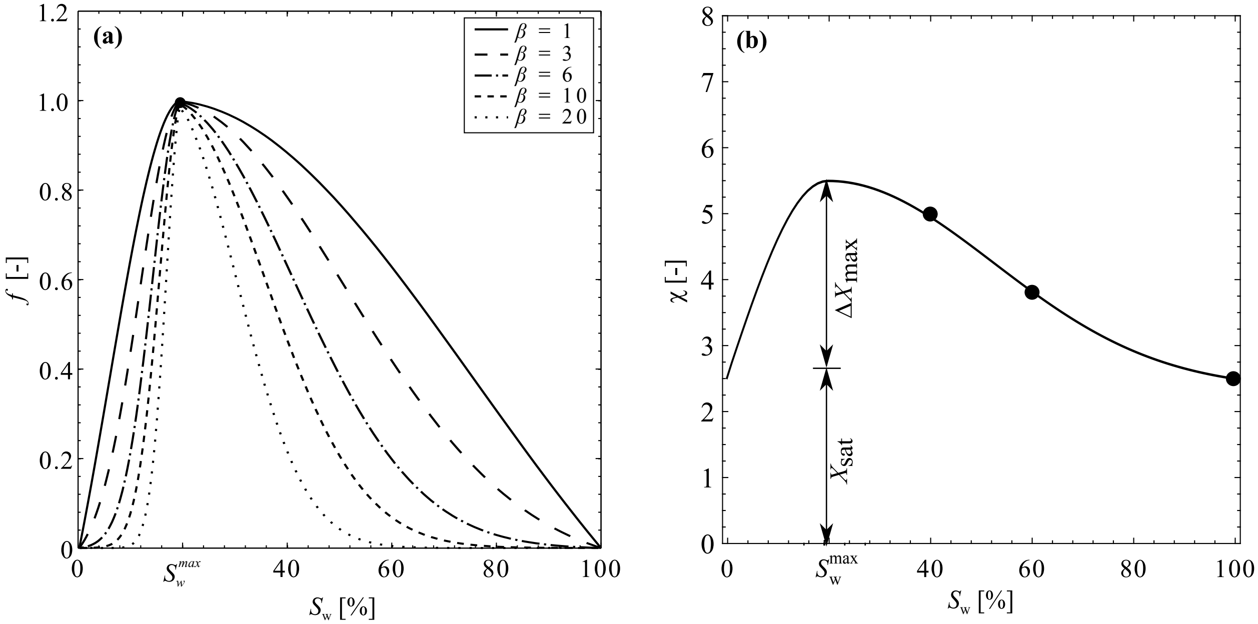

Figure9

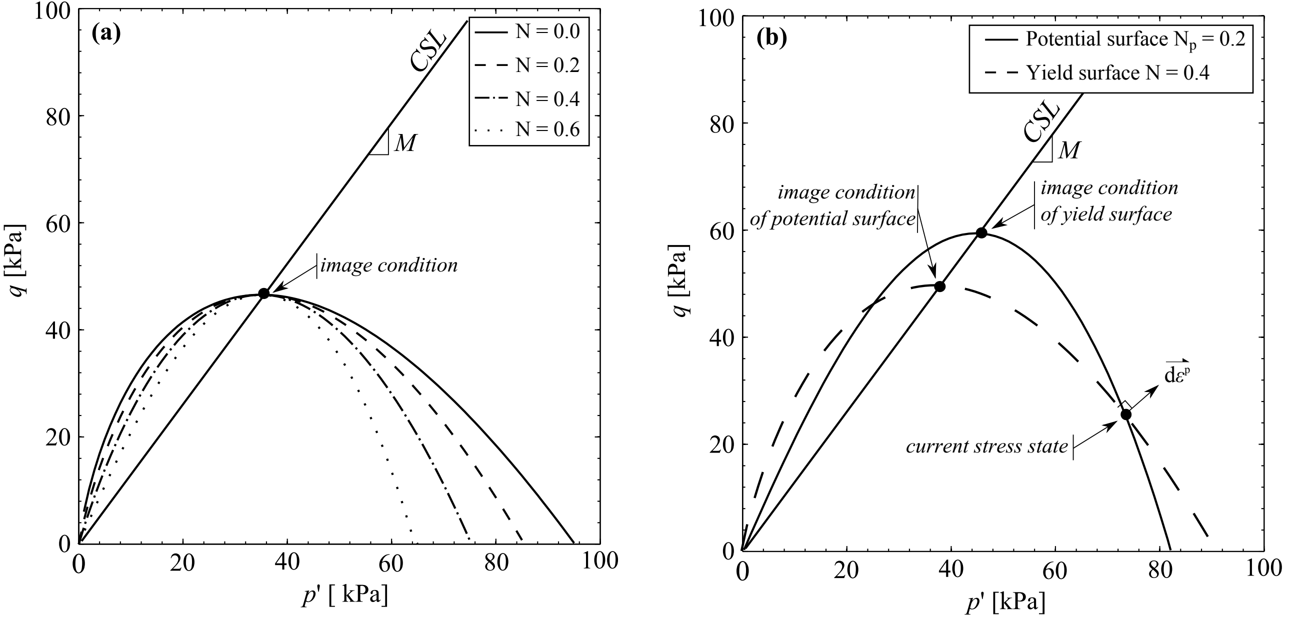
(a)
N = 0.0
N = 0.2
N = 0.4
N = 0.6
CSL
M
image condition
q [kPa]
p' [kPa]
0
20
40
60
80
100
(b)
Potential surface N_p = 0.2
Yield surface N = 0.4
CSL
M
image condition of potential surface
image condition of yield surface
dε^p
current stress state
q [kPa]
p' [kPa]

Figure10 Click here to download Figure Fig10.pdf

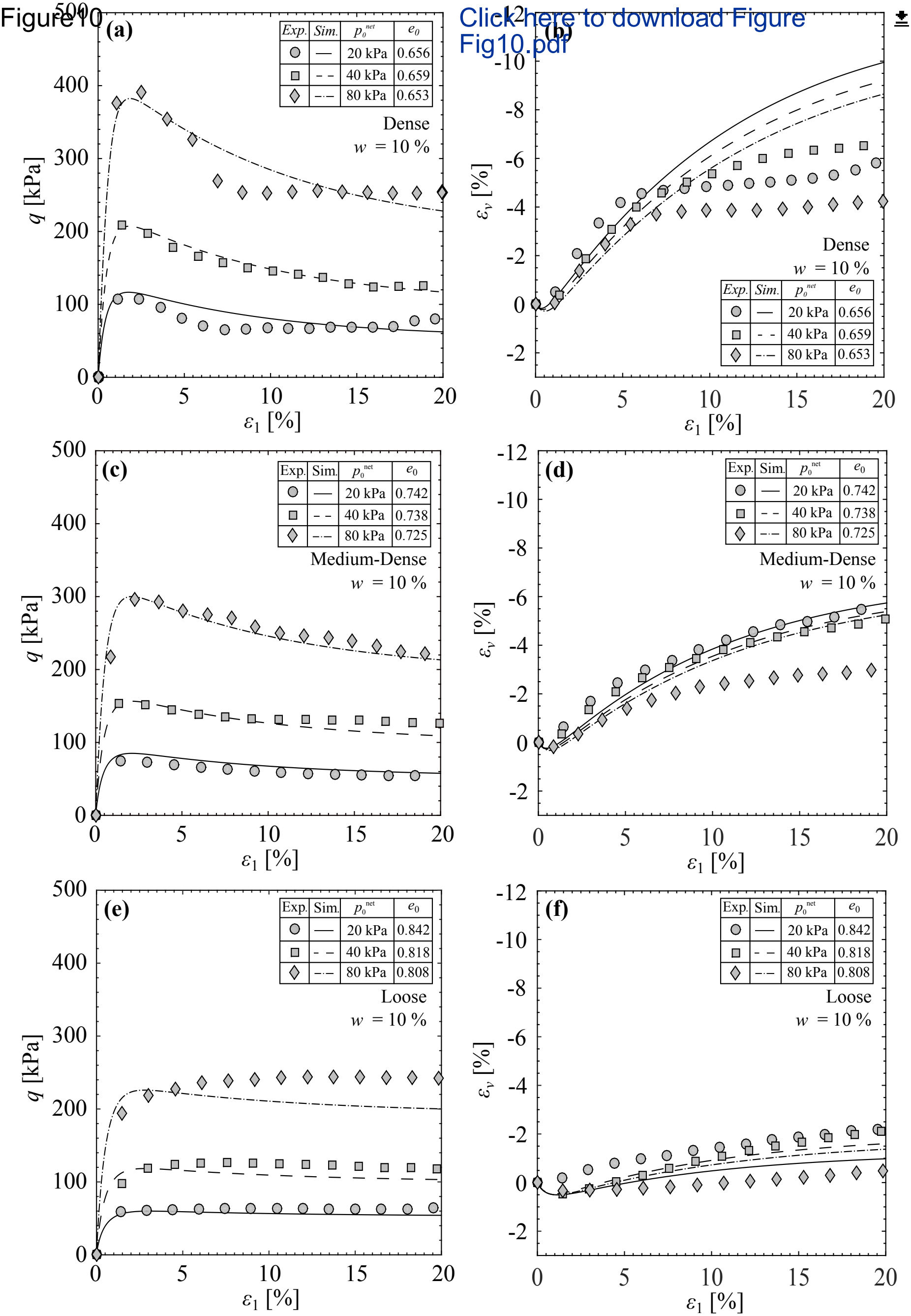

Figure 11

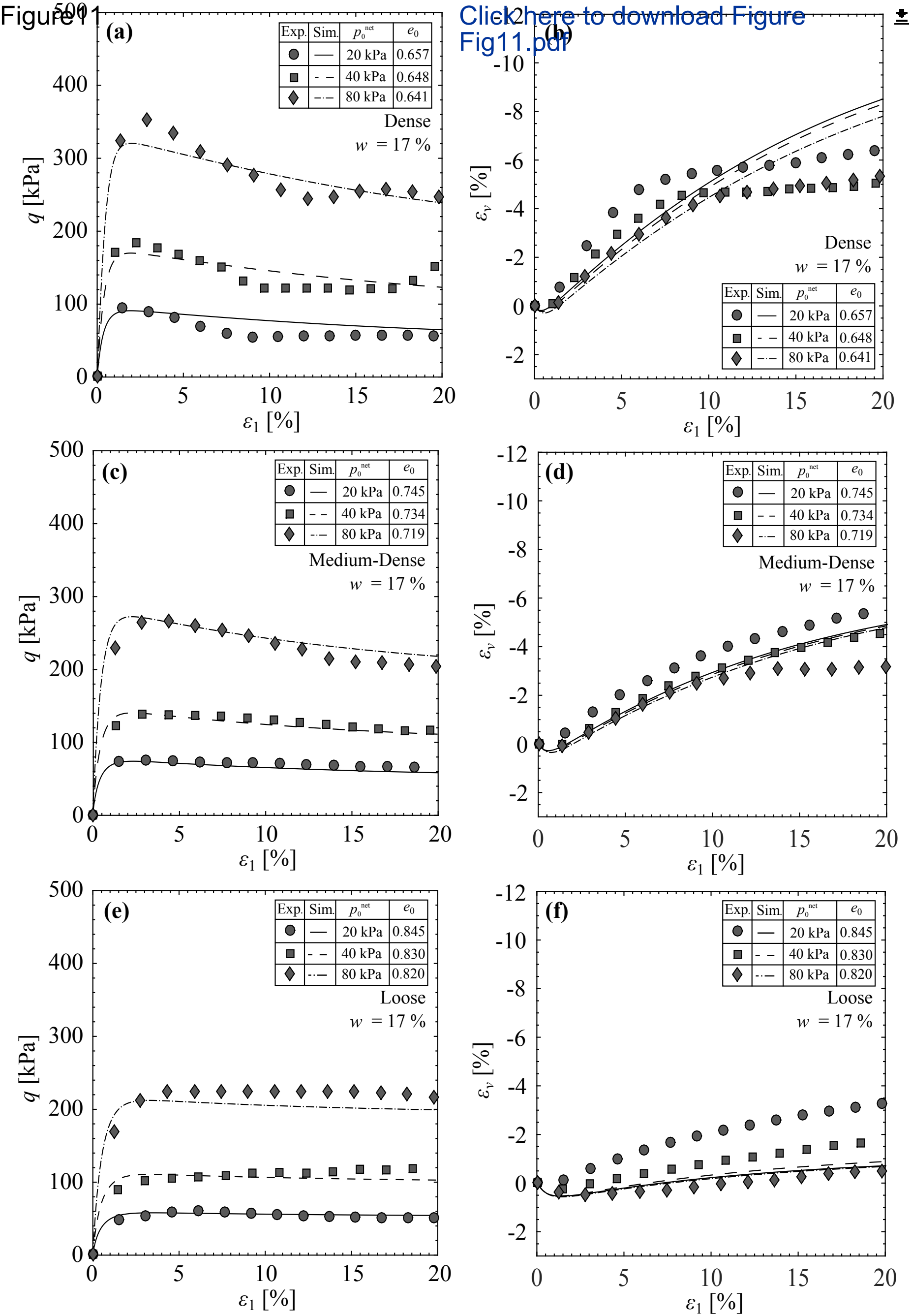

(a)
(b)
(c)
(d)
(e)
(f)
Exp. Sim. p_0^{net} e_0
20 kPa 0.657
40 kPa 0.648
80 kPa 0.641
20 kPa 0.745
40 kPa 0.734
80 kPa 0.719
20 kPa 0.845
40 kPa 0.830
80 kPa 0.820
Dense
Medium-Dense
Loose
w = 17 %
q [kPa]
ε_v [%]
ε_1 [%]

Figure12

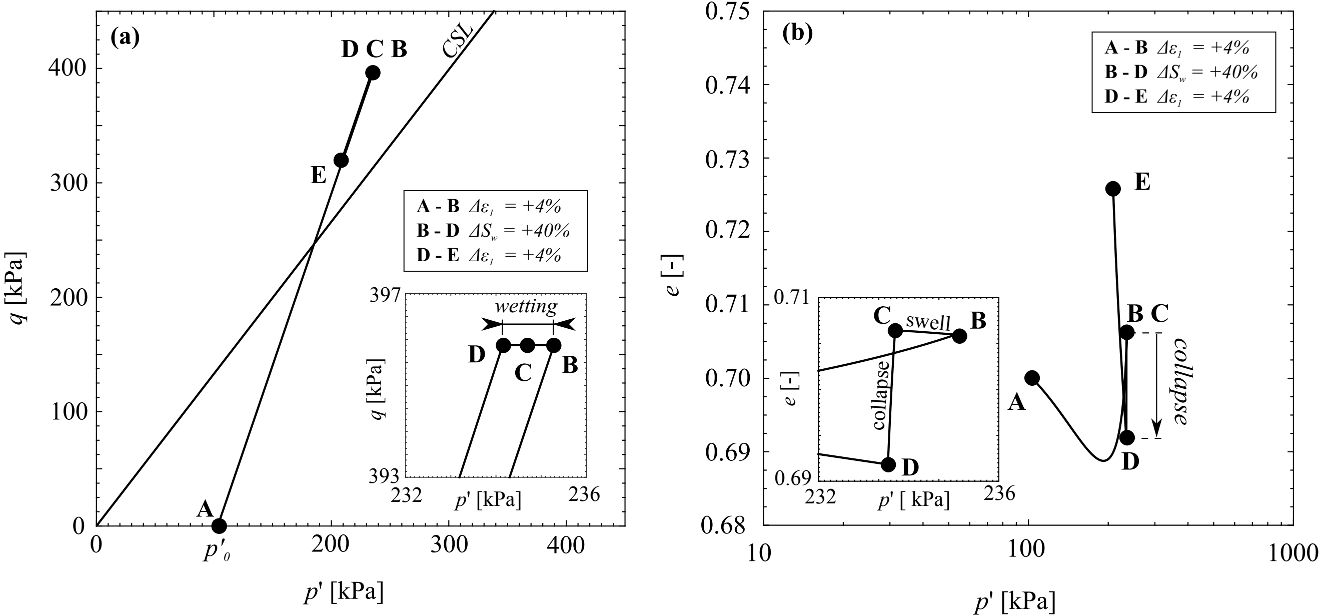

(a)
D C B
CSL
E
A
A - B Δε1 = +4%
B - D ΔSw = +40%
D - E Δε1 = +4%
q [kPa]
p' [kPa]
p'0
0
100
200
300
400
wetting
D
C
B
397
393
232
236
(b)
A - B Δε1 = +4%
B - D ΔSw = +40%
D - E Δε1 = +4%
E
B C
collapse
A
D
e [-]
p' [kPa]
0.68
0.69
0.70
0.71
0.72
0.73
0.74
0.75
10
100
1000
C
swell
B
collapse
D
0.71
0.69
232
236
p' [kPa]

Figure13

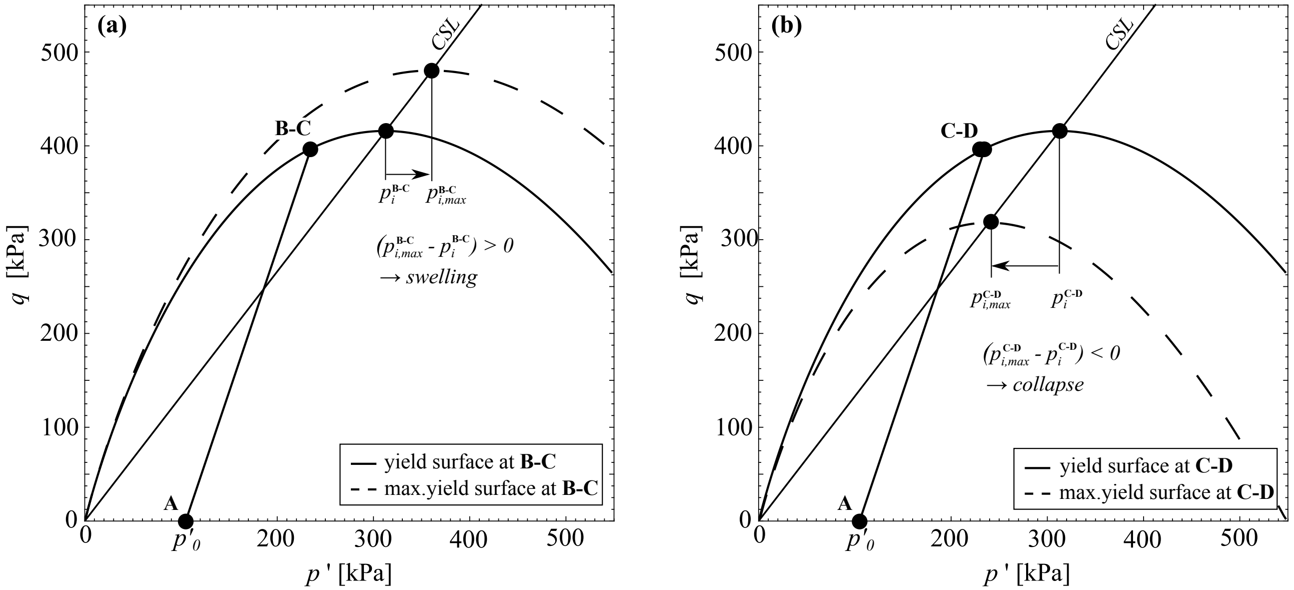
(a)
CSL
B-C
A
p_i^{B-C}
$p_{i,max}^{B-C}$
$(p_{i,max}^{B-C} - p_i^{B-C}) > 0$
→ swelling
yield surface at **B-C**
max.yield surface at **B-C**
q [kPa]
p ' [kPa]
p'_0
(b)
CSL
C-D
A
$p_{i,max}^{C-D}$
p_i^{C-D}
$(p_{i,max}^{C-D} - p_i^{C-D}) < 0$
→ collapse
yield surface at **C-D**
max.yield surface at **C-D**
q [kPa]
p ' [kPa]
p'_0